Journal of Molecular Structure 1223 (2021) 129240

Contents lists available at ScienceDirect

Journal of Molecular Structure

journal homepage: www.elsevier.com/locate/molstr

Tetraacuo-bis-(N,N-dimethylacetamide-O)magnesium(II) chloride dihydrate. An option to improve magnesium effect on phosphatase stimulation and albumin binding

Nancy Martini[a], Juliana E. Parente[a], Gonzalo Restrepo-Guerrero[a], Carlos A. Franca[a], Oscar E. Piro[b], Gustavo A. Echeverría[b], Patricia A.M. Williams[a], Evelina G. Ferrer[a,*]

[a] Centro de Química Inorgánica (CEQUINOR-CONICET-CICPBA-UNLP)-Departamento de Química- Facultad de Ciencias Exactas, Universidad Nacional de La Plata, Boulevard 120 entre 60 y 64, C.C.962- (B1900AVV), 1900 La Plata, Argentina
[b] Departamento de Física, Facultad de Ciencias Exactas, Universidad Nacional de La Plata and IFLP (CONICET, CCT-La Plata), C.C. 67, 1900 La Plata, Argentina

ARTICLE INFO

Article history:
Received 18 July 2020
Revised 9 September 2020
Accepted 9 September 2020
Available online 10 September 2020

Keywords:
Magnesium
N,N-dimethylacetamide
ALP stimulation
Albumin interaction

ABSTRACT

Magnesium compounds became relevant since the discovery that this element is essential and its deficiency causes several diseases. From these findings, magnesium supplementation became a pharmacologically important issue that prompted the search for new drugs. There are many commercial formulations for restoring electrolyte balance, nutrition, learning, Alzheimer's disease, mood disorder, pain, etc. Magnesium is found in ALP and is known to be able to stimulate its activity. Because of that, there is a great interest in a study of the activity of magnesium compounds as a drug for osteoporosis. Metal complexes are known to improve the bioavailability and the pharmacological performance of drugs. Thus, we combine the pharmacological ability of magnesium together with the potential biological activity of N,N-dimethylacetamide (a common solvent used in pharmaceutical preparations). The present study reports the chemical syntheses of $[Mg(DMA)_2(H_2O)_4]Cl_2.2H_2O$ complex and the clinical potential implication as phosphatase stimulator. In a typical phosphatase assay containing p-nitrophenyl phosphate, the kinetic constants (K_m and K_{cat}) were calculated through Michaelis-Menten assumptions and the activities of the magnesium complex, alkaline phosphatase and magnesium chloride had been compared. The compound can activate ALP hence suggesting that it could regulate bone matrix formation. Albumin binding experiments were also performed and revealed a better interaction than the well-known magnesium chloride salt.

1. Introduction

Magnesium is an essential element and the main biologically available sources are the oceans and rivers. It dissolves easily and binds water molecules tighter than other elements like calcium, potassium, and sodium. The total magnesium content in an adult human body (70 kg) is approximately 1 mol. About 99% is located in bones, muscles, and non-muscular soft tissues. Its intracellular content ranges from 1 to 5% and it binds to negatively-charged molecules, proteins, and adenosine triphosphate (ATP). The extracellular percentage of Mg^{2+} is 1% and it is found in serum and red blood cells. Magnesium acts as a cofactor in enzymatic reactions stabilizing enzymes and it is involved in ATP production. Its metabolism influences the glucose-intervening process, synthesis of fat, proteins, nucleic acids, muscle contraction, and many others. It additionally contributes to normal neurological function and the release of neurotransmitters. Due to its biological relevance, magnesium deficiency is a potential health risk associated with several diseases. Deficiency symptoms are anorexia, nausea, vomiting, lethargy, weakness, paresthesia, muscular cramps, irritability, decreased attention span, and mental confusion [1]. There are many commercial magnesium supplements to restore the normal levels [2].

There is also a growing interest in the effects that magnesium may produce on the activity of alkaline phosphatase (ALP). This enzyme generated by osteoblasts is essential in tissue formation. It catalyzes the cleavage of the ester group of p-nitrophenyl phosphate (PNPP) into p-nitrophenol (PNP). In bone formation, high ALP enzyme levels are an early marker of osteoblastic differentiation and mineralization. In this sense, the increment of its activ-

* Corresponding author.
E-mail address: evelina@quimica.unlp.edu.ar (E.G. Ferrer).

https://doi.org/10.1016/j.molstruc.2020.129240
0022-2860/

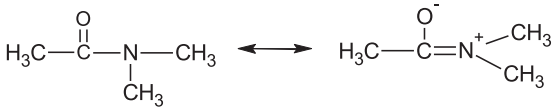

Fig. 1. Resonance structures of N,N-dimethylacetamide (DMA).

ity provides therapeutic opportunities for the treatment of bone diseases and also the creation of bone biomaterials [3]. Different, but few experiments are found in the literature regarding ALP levels including magnesium compounds. Magnesium is also important in bone regeneration. This bio-essential element influences the final composition and the bone-crystal structure. Its deficiency is involved in osteoporosis. It was shown that Mg^{2+} could be adsorbed or retained on the surface or inside of hydroxyapatite to be released during bone resorption [4]. Intra-peritoneal injection of MgO-nanoparticles in Wistar rats, especially in doses ranging from 125 $\mu g.mL^{-1}$ to 250 $\mu g.mL^{-1}$, considerably increases ALP activity [5]. $MgCl_2$ enhances the rate of hydrolysis of PNPP by ALP in a concentration-dependent manner [6]. Its deprivation reduced calf intestinal alkaline phosphatase activity with a K_m value ranging from ~0.25 mM to ~0.03 mM.

The activity of ALP in UMR106 osteosarcoma cells was also inhibited 30% by Mg^{2+} deficiencies [7]. It is known that different compounds of the same element could demonstrate non-identical results in biological assays. Several factors may be involved in these behaviors such as the differences in structure, charge factors, physical, and pharmacological properties allowing the compound to be released or to be achieved in a certain location where it is needed. $MgSO_4$ and $MgCl_2$ have dissimilar pharmacological and toxicological properties being the absorption and retention of the chlorine more efficient [8]. Certainly, in vivo studies with albino male Wistar rats fed with $MgSO_4$ (0.06 mg/mL, 12 weeks) did not show any significant effect on the activity of ALP extracted by femoral diaphysis [4].

On the other side, N,N-dimethylacetamide (DMA, Fig. 1) is a potent industrial solvent and also an intermediate for many organic reactions in the synthesis of agrochemicals, pharmaceuticals, and fine chemicals. This solvent is very convenient for the dissolution of polyacrylonitrile, polyimides, cellulose derivative, polyvinyl chloride, polyamides, styrenes, and linear polyesters. It is also used as a vehicle in pharmaceutical formulations (tetracycline, oxytetracycline, chloramphenicol, amsacrine, diaziquone, triazineantifolate, myleran, and teniposide). Considering that this solvent possesses manageable toxicity (for example in amsacrine-DMA lactate formulation DMA ranged between 57.3-159.4 g for patients with a bodyweight of 70 kg), it seems to be a suitable ligand for other pharmacological applications [9]. There are several reports in the literature on metal complexes using this solvent as a ligand [10–12] but their pharmacological use has not yet been described.

Another important factor concerning the bioavailability of the biological relevant compound is the capacity to be transported by serum proteins. Serum albumin is the main circulating protein involved in controlling levels of Mg^{2+}. Different experiments and techniques led to a similar result: magnesium binds to albumin with a dissociation constant of ~10^2-10^3, and no significant changes are observed in the fluorescence emission spectrum of BSA [13,14]. However, the bioavailability of the new compound could be evaluated by fluorescence spectroscopy measurements.

These results prompt us to study the potential synergistic effects on ALP and albumin interaction ability produced by the new coordination complex, tetraacuo-bis-(N,N-dimethylacetamide-O)magnesium(II) chloride dihydrate (MgDMA) and to compare the effects with those produced by $MgCl_2$.

2. Materials and methods

All chemicals used were of analytical grade. The hexahydrate salts of magnesium nitrate and chloride were obtained from Biopack and N,N-dimethylacetamide from Anedra. Elemental analyses for carbon, hydrogen and nitrogen were performed using a Carlo Erba EA 1108 analyzer. FTIR absorption spectra of powdered samples sandwiched between KBr disks were measured with a Bruker IFS 66 FTIR-spectrophotometer from 4000 to 400 cm^{-1}. Raman dispersion spectra were collected on a Raman Horiba JobinYvon T64000 (confocal microscopy Olympus BX41) spectrophotometer with a laser power of 400 and 800 mW (Ar, 514.5 nm) and at a spectral resolution of 4 cm^{-1}. Each spectrum was obtained as an average of 10 scans collected in the 4000-400 cm^{-1} range.

UV-Vis and reflectance spectra determinations were recorded with a Shimadzu 2600/2700 spectrophotometer. Fluorescence spectra were obtained using a Shimadzu (RF6000) luminescence spectrometer equipped with a pulsed xenon lamp. The three-dimensional fluorescence spectra were obtained using a Perkin Elmer (Beaconsfield, UK) LS-50B luminescence spectrometer equipped with a pulsed xenon lamp (half peak height b10 μs, 60 Hz) and R928 photomultiplier tube and the data has been processed with FLWinlab software. The experimental conditions were: (i) Emission wavelength was recorded between 200 and 600 nm, (ii) Excitation wavelength from 200 to 400 (5 nm of increment), (iii) the number of scanning curves was 15, (iv) Scan speed: 6000 nm/min, (v) Bandwidth: 3 nm.

2.1. Synthesis of $[Mg(DMA)_2(H_2O)_4]Cl_2.2H_2O$ (MgDMA)

The magnesium complex was prepared by direct reaction between magnesium chloride hexahydrate salt and N,N-dimethylacetamide. For the synthesis of the complex, 2 mmol of $MgCl_2.6H_2O$ were added to a magnetically stirred solution containing 1 mmol of hot N,N-dimethylacetamide (10 mL). After refluxing at 100 °C for 2 h under continuous stirring, the resulting solution was left to stand for 48 h. The colorless single crystals formed that resulted suitable for structural X-ray diffraction determinations, were filtered off, washed with N,N-dimethylacetamide, and air-dried. Yield: 80-88%.

Elemental analyses for C, H, N confirm the composition: $C_8H_{30}Cl_2MgN_2O_8$: Calculated: 25.43 %C, 7.95 %H, 7.42 %N; Found: 25.50% C, 7.87%H, 7.48 % N.

2.2. Crystal data and structure solution and refinement

The measurements were performed on an Oxford Xcalibur Gemini, Eos CCD diffractometer with graphite-monochromatedMoKα (λ = 0.71073 Å) radiation. X-ray diffraction intensities were collected (ω scans with ϑ and κ-offsets), integrated and scaled with CrysAlisPro [15] suite of programs. To avoid degradation, the crystal was mounted on the goniometer head embedded in an oil droop. The unit cell parameters were obtained by least-squares refinement (based on the angular settings for all collected reflections with intensities larger than seven times the standard deviation of measurement errors) using CrysAlisPro. Data were corrected empirically for absorption employing the multi-scan method implemented in CrysAlisPro.

The structure was solved by intrinsic phasing with SHELXT [16] and refined with anisotropic displacement parameters for the non-H atoms with SHELXL program of the SHELX package [17]. All H-atoms were found in a difference Fourier map phased on the heavier atoms and refined at their found positions with isotropic displacement parameters. Crystal data, data collection procedure, and refinement results are summarized in Table 1.

Table 1
Crystal data and structure refinement for $[Mg(DMA)_2(H_2O)_4]Cl_2.2H_2O$ (MgDMA).

Empirical formula	$C_8H_{30}Cl_2MgN_2O_8$
Formula weight	377.55
Temperature	297(2) K
Wavelength	0.71073 Å
Crystal system	Monoclinic
Space group	I 2/a
Unit cell dimensions	a = 16.4182(8) Å b = 8.0355(4) Å c = 29.573(2) Å β = 91.376(5)°
Volume	3900.4(3) Å3
Z	8
Density (calculated)	1.286 Mg/m3
Absorption coefficient	0.396 mm-1
F(000)	1616
Crystal size	0.386 × 0.253 × 0.244 mm3
ϑ-range for data collection	3.154 to 28.868°
Index ranges	$-21 \le h \le 21$, $-10 \le k \le 8$, $-36 \le l \le 40$
Reflections collected	9693
Independent reflections	4282 [R(int) = 0.0276]
Observed reflections [$I>2\sigma(I)$]	2191
Completeness to ϑ = 25.242°	99.7 %
Refinement method	Full-matrix least-squares on F2
Data / restraints / parameters	4282 / 1 / 245
Goodness-of-fit on F2	1.002
Final R indices [$I>2\sigma(I)$]	R1 = 0.0473, wR2 = 0.1299
R indices (all data)	R1 = 0.0927, wR2 = 0.1689
Largest diff. peak and hole	0.271 and -0.308 e.Å-3

[a] $R_1=\Sigma||F_o|-|F_c||/\Sigma|F_o|$, $wR_2=[\Sigma w(|F_o|^2-|F_c|^2)^2/\Sigma w(|F_o|^2)^2]^{1/2}$.

2.3. Hirshfeld surface analysis (HSs)

Hirshfeld surface analysis (HSs) was performed using Crystal Explorer 3.1 [18], based on structural single-crystal X-ray diffraction studies. The function d_{norm} is the ratio including the distances of any surface point to the nearest interior (d_i) and exterior (d_e) atom and the van der Waals radii of the atoms. When the d_{norm} function has a negative value, it indicates that the sum of d_i and d_e is less than the sum of the relevant van der Waals radii and it is considered to be a close contact. In the map of HSs, the closest contacts appear in red, the intermolecular distances (near to van der Waals contacts with d_{norm} = 0) in white color and the contacts which are longer than the sum of van der Waals radii (positive d_{norm} values) are blue-colored. The presence of different types of intermolecular interactions can be observed in a 2D fingerprint plot of d_i versus d_e.

2.4. Computational methods

The input data for the computational calculations were taken from crystallographic parameters obtained for MgDMA. The optimization of the geometries and the vibration analysis for the magnesium complex were carried out to get the lowest value in the potential energy surface. The calculations were performed with the Density Functional Theory tools as implemented in GAUSSIAN 09 [19], using the hybrid functional with non-local exchange due to Becke [20] and the correlation functional due to Parr [21] known as B3LYP. Contracted Gaussian basis sets of triple-zeta quality plus polarized and diffuse functions 6-311++g(2d,p) [22] for all atoms were used throughout the present work. The corresponding vibration analyses were performed for the optimized geometry to verify whether it is a local minimum or saddle point on the potential energy surface of the molecule. The calculations were also carried out with the Gaussian 09 package. Calculated normal modes were also used to assist the assignment of experimental frequencies.

The electronic spectra of the compounds were calculated using the time-dependent density functional theory [23] as implemented in the Gaussian 09 package. The vertical transition energies were calculated at the optimized ground-state geometry using the meta-hybrid PBE0 functional [24] to produce a number of 80 singlet-to-singlet transitions. Solvent effects (water) were also included at the same level of theory using the Polarizable Continuum Model [25].

2.5. Phosphatase activity

The conversion of the substrate *p*-nitrophenyl phosphate (PNPP) to *p*-nitrophenol (PNP) was monitored by the absorbance changes at 405 nm (ε = 18500 $M^{-1}.cm^{-1}$). The experimental conditions for ALP specific activity measurement were: 1 μg/mL of bovine intestinal ALP (6.25×10^{-6} mM) and PNPP (with final concentrations ranging from 0.04 to 0.4 mM) were dissolved in the incubation buffer (55 mM glycine + 0.55 mM $MgCl_2$, pH=10.4) and held for 5 min at 37 °C. The effects of the compounds were determined by the addition of different volumes of 5 mM $MgCl_2$ and MgDMA to the pre-incubated mixture. The effect of each concentration was repeated five times in three different experiments.

2.6. Evaluation of the catalytic parameters

A treatment based on the Michaelis-Menten model developed for enzyme kinetics studies was performed. The values of the Michaelis binding constant (K_m), maximum velocity (V_{max}), and rate constant for dissociation of substrates (i.e., turnover frequency, k_{cat}) were calculated from the Lineweaver-Burk graph (double reciprocal plot) of 1/rate versus 1/[S], using the equation $1/V = (K_m/V_{max})(1/[S]) + 1/V_{max}$. A control reaction carried out without the magnesium complex shows no change in the absorbance at 405 nm. The data represent triplicate determinations and were performed at least five times.

2.7. Albumin interaction

2.7.1. Fluorescence quenching experiments

Bovine serum albumin (BSA) was dissolved in 0.1M Tris-HCl buffer (pH 7.4) to attain a final concentration of 6 μM. The solutions of the studied compounds were added drop-wise to the above preparation to ensure the formation of a homogeneous solution and to obtain the desired concentration of 0-1000 μM. Adequate solubility was reached under these experimental conditions and the compounds did not show significant fluorescence that could interfere with the measurements. For each sample and concentration, three independent replicates were performed at 25 °C and 37 °C. BSA 6 μM was titrated by successive additions of complex solutions from 0 to 1000 μM and the fluorescence intensity was measured (excitation at 280 nm and emission at 348 nm). All the fluorescence quenching data were analyzed according to previous studies performed in the laboratory by applying a traditional mathematical procedure. The fluorescence-quenching mechanism has been analyzed using the Stern-Volmer Eq. (1), [26]

$$F^0/F = 1+K_{sv}[Q] \quad (1)$$

where F^o is the steady-state fluorescence intensity of BSA alone while F is the observed intensity upon increasing the quencher concentration, K_{sv} is the Stern-Volmer quenching constant and [Q] is the quencher concentration. Usually, the curve of F^o/F *vs* [Q] is linear if the type of quenching involves a unique process: either static or dynamic. Static quenching is due to the complex formation between the fluorophore and the quencher. It can be distinguished from collision effects when the K_{sv} value results higher than the value of the dynamic quenching constant (K_q). Considering that $K_q = K_{sv}/\tau_0$ (where τ_0, 10^{-8} s, is the average lifetime of the bio-molecule without quencher), this constant can be estimated and compared with the maximum diffusion collision quenching rate constant (reference value from the literature) which

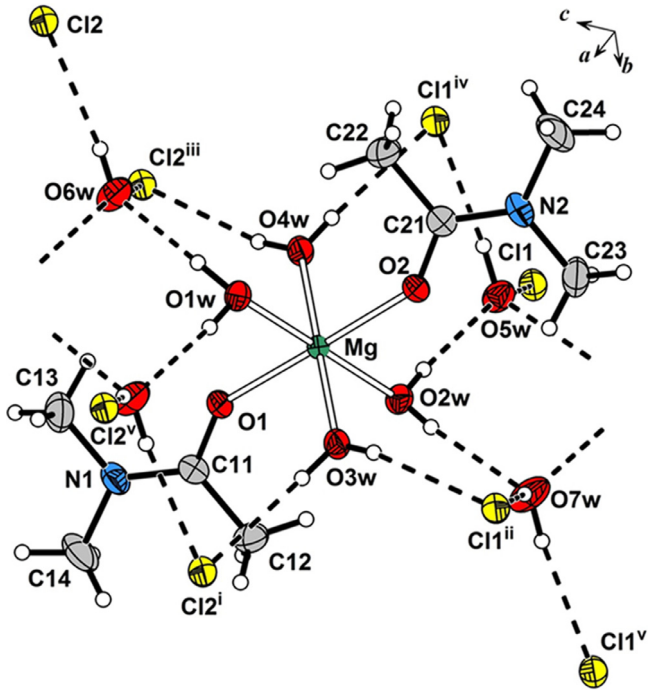

Fig. 2. View of $[Mg(DMA)_2(H_2O)_4]Cl_2.2H_2O$ (MgDMA) showing the labeling of the non-H atoms and their displacement ellipsoids at the 30% probability level. Ligand-metal bonds are indicated by open lines and H-bonds by dashed lines. Symmetry operations: (i) -x+1/2, -y+3/2, -z+3/2; (ii) -x+1/2, y+1, -z+1; (iii) -x+1/2, -y+1/2, -z+3/2; (iv) -x+1/2, y, -z+1; (v) x, y+1, z.

is 2×10^{-10} $M^{-1}s^{-1}$ [26]. If K_{sv} resulted greater, then a mechanism of interaction by complex formation can be proposed. Otherwise, it would be a collisional quenching. If the quenching is static, it is assumed that there are specific binding sites. These binding sites and their association constants could be estimated using the following mathematical relationship:

$$\log\left[\left(F^0-F\right)/F\right] = \log K_b + n\log[Q] \quad (2)$$

where K_b is the binding constant and n is the average number of the binding site per protein molecule.

To obtain information about the type of interaction, the thermodynamic parameters were calculated using the Vant́ Hoff equation:

$$\ln(K_{b2}/K_{b1}) = -\Delta H^0/R(1/T_2-1/T_1) \quad (3)$$

where T_1 and T_2 are the absolute temperatures at which K_{b1} and K_{b2} were determined. The standard free energy change (ΔG^0) and the standard free entropy change (ΔS^0) were evaluated according to the well-known thermodynamic relationships:

$$\Delta G^0 = -RT\ln K_b \quad (4)$$

$$\Delta S^0 = \left(\Delta H^0-\Delta G^0\right)/T \quad (5)$$

3. Results and discussion

3.1. Structural results and Hirshfeld surface analysis

Fig. 2 is an ORTEP [27] drawing of $[Mg(DMA)_2(H_2O)_4]Cl_2.2H_2O$ salt and bond distances and angles around the metal are listed in Table 2. The Mg^{2+} ion is in an almost perfect octahedral environment (MgO_6), equatorially coordinated to four water molecules [Mg-Ow bond distances from 2.055(2) to 2.100(2) Å] and axially to the carbonyl oxygen atoms of two DMA ligands [Mg-O bond lengths of 2.041(2) and 2.042(2) Å]. *Trans* O-Mg-O bond angles are in the range from 179.12(7) to 179.50(9)° and *cis* O-Mg-O angles are in the 87.29(9)-92.83(7)° interval. DMA ligands are nearly coplanar with each other [angled at 4.1(2)°], perpendicular to the equatorial plane [dihedral angle of 85.02(5)°], and tilted with respect to the axial O1wO2wO1O2 coordination plane in 32.91(5)°.

Table 2
Bond lengths [Å] and angles [°] around the metal in $[Mg(DMA)_2(H_2O)_4]Cl_2.2H_2O$.

Mg-O(1)	2.041(2)
Mg-O(2)	2.042(2)
Mg-O(1W)	2.097(2)
Mg-O(2W)	2.100(2)
Mg-O(3W)	2.055(2)
Mg-O(4W)	2.058(2)
O(1)-Mg-O(2)	179.12(7)
O(1)-Mg-O(3W)	90.44(8)
O(2)-Mg-O(3W)	90.30(8)
O(1)-Mg-O(4W)	89.41(8)
O(2)-Mg-O(4W)	89.86(8)
O(3W)-Mg-O(4W)	179.3(1)
O(1)-Mg-O(1W)	87.29(9)
O(2)-Mg-O(1W)	92.23(9)
O(3W)-Mg-O(1W)	89.81(8)
O(4W)-Mg-O(1W)	90.84(8)
O(1)-Mg-O(2W)	92.83(9)
O(2)-Mg-O(2W)	87.66(9)
O(3W)-Mg-O(2W)	89.70(9)
O(4W)-Mg-O(2W)	89.65(9)
O(1W)-Mg-O(2W)	179.50(9)

The crystal is arranged as electrically neutral layers $a/2$ in thickness parallel to (100) plane. Neighboring layers are symmetry-related by mirror glide planes along the a-axis and linked to each other through intercalated DMA ligands (see Fig. 3). The crystal is further stabilized by a rich intra-layer H-bonding structure involving the water molecules (see Fig. 2). These can be grouped into two sets; one of them includes the four coordination water molecules (w1-w4), the other one the three crystallization water molecules (w5-w7), with the O5w and O7w oxygen atoms sited at crystallographic two-fold axes. All coordination waters in the first set act as a donor in OwH…A bonds: w1 and w2 are H-bonded to the water molecules of the other set acting as acceptors [OwH…Ow bond distances from 1.90(4) to 2.04(3) Å and Ow-H…Ow bond angles in the 165(3)-176(3)° range]; w3 and w4 are H-bonded to chlorine ions [OwH…Cl distances from 2.34(3) to 2.43(3) Å and Ow-H…Cl angles in the 166(2)-175(3)° range]. The crystallization water molecules of the second set also act as donors in OwH…Cl bonds [OwH…Cl distances from 2.25(3) to 2.36(3) Å and Ow-H…Cl angles in the 171(3)-174(3)° range]. The OwH…A bonding structure is detailed in Table 3.

In addition to crystallographic data (Table 3), the intermolecular interactions were analyzed by HSs. Fig. 4 discloses the close contacts of hydrogen bond donors and acceptors. Dominant contacts can be seen as intense circular red spots in the d_{norm} surface associated with hydrogen atoms belonging to coordinated water molecules with oxygen atoms from the crystallization water molecules (Fig. 4A). These directional hydrogen-bonding interactions (H(inside)…O(outside)) together with the hydrogen-chlorine (H(inside)…..Cl(outside)) contribute with 8.6% and 10.8% of the total Hirshfeld surface with two spikes in the 2D fingerprint plot (Fig. 4B and C).The non-directional H…..H contacts are characterized by broader spikes (Fig. 4D). It is known that crystal lattice strength can be estimated according to the H…H close contacts. Usually, the percentage of the Hirshfeld area with H…H contacts is higher than the other contacts because of the small atomic volume of hydrogen [28]. In this crystal, the contribution is 73.1% with few contacts with distances shorter than 2.32 Å (<sum of atomic radii)

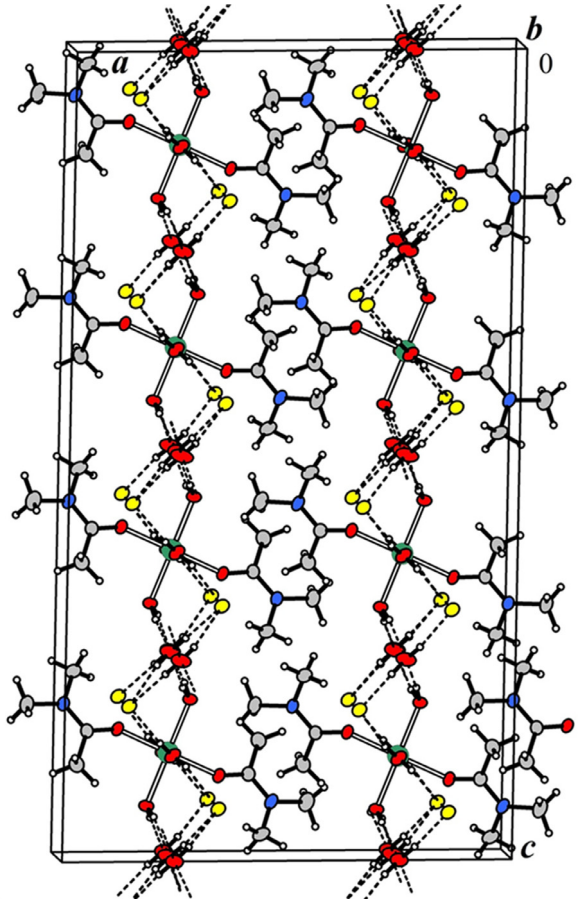

Fig. 3. Crystal packing of $[Mg(DMA)_2(H_2O)_4]Cl_2.2H_2O$ (MgDMA) as seen down the *b*-axis showing the layered structure parallel to (100) plane. Magnesium, oxygen, nitrogen, and chlorine atoms are in green, red, blue and yellow colors, respectively.

Table 3
Hydrogen bond distances [Å] and angles [°] for $[Mg(DMA)_2(H_2O)_4]Cl_2.2H_2O$.

D-H...A	d(D-H)	d(H...A)	d(D...A)	∠(D-H...A)
O(1W)-H(1A)...O(6W)#1	0.77(3)	2.06(3)	2.821(3)	172(3)
O(1W)-H(1B)...O(6W)	0.90(4)	1.90(4)	2.789(3)	176(3)
O(2W)-H(2A)...O(5W)	0.77(3)	2.02(4)	2.791(3)	174(4)
O(2W)-H(2B)...O(7W)	0.79(3)	2.04(3)	2.814(3)	165(3)
O(3W)-H(3A)...Cl(2)#1	0.82(3)	2.34(3)	3.161(2)	175(3)
O(3W)-H(3B)...Cl(1)#2	0.74(3)	2.43(3)	3.153(2)	168(3)
O(4W)-H(4A)...Cl(2)#3	0.83(3)	2.35(3)	3.155(2)	166(2)
O(4W)-H(4B)...Cl(1)#4	0.77(3)	2.42(3)	3.181(2)	175(3)
O(5W)-H(5)...Cl(1)	0.91(3)	2.25(3)	3.154(2)	174(3)
O(6W)-H(6A)...Cl(2)#3	0.89(3)	2.29(3)	3.182(2)	173(3)
O(6W)-H(6B)...Cl(2)	0.82(3)	2.34(4)	3.155(2)	171(3)
O(7W)-H(7)...Cl(1)#5	0.83(3)	2.36(3)	3.183(2)	172(3)

Symmetry transformations used to generate equivalent atoms: (#1) -x+1/2, -y+3/2, -z+3/2; (#2) -x+1/2, y+1, -z+1; (#3) -x+1/2, -y+1/2, -z+3/2; (#4) -x+1/2, y, -z+1; (#5) x, y+1, z.

and more contacts with distances larger than 2.57 Å. As a consequence of those contributions, a low melting point was expected for the magnesium complex. In fact, it was observed at the low temperature value of 95 ± 0.1 °C, in agreement with reported values [28].

3.2. Physicochemical characterization

FTIR and Raman spectra of the magnesium complex were analyzed by comparison with the free ligand and the vibrational assignments were assisted by DFT calculations (Table S6). Experimental and theoretical FTIR spectra of $[Mg(DMA)_2(H_2O)_4]Cl_2.2H_2O$ are compared in Fig. 5 along with the experimental spectrum of DMA. It can be appreciated that the experimental and the selected calculated frequencies for the compound are in good agreement with each other even without the use of scaling factors.

The vibration spectra of N,N-dimethylacetamide has been extensively studied [29]. The characteristic DMA band located at 1652 cm^{-1} has contributions of C=O and C≡N) stretching vibrations. It is known that the DMA structure can be described as a resonance hybrid. When metal coordination occurs, and DMA is present in the protonated form, a decrease in the C-O bond order and an increase in the CN bond order are expected. The vibrational determinations allow us to confirm that this is the structure of DMA upon coordination to the magnesium ion in $[Mg(DMA)_2(H_2O)_4]Cl_2.2H_2O$ (Figs. 1, 2) and the expected lowering of the C=O band and the increment of the C≡N are observed at 1626 cm^{-1} and 1524 cm^{-1}, respectively (Table S6, Fig. 5). Upon coordination the bands of DMA located at 1265 cm^{-1} and 1190 cm^{-1}, respectively, assigned to the asymmetric CN stretching mode and the combination vibration mode of νCC and NCH_3 rock, are blue-shifted to 1272 and 1200 cm^{-1}. Contrasting with DMA, the set of bands of the complex in the 1065-1030 cm^{-1} range have contributions of vibration modes involving HCNC, NC and CNOC groups. On the other side, the sensitive band found at 591 cm^{-1} in DMA, assigned to the bending mode of the OCN group, appears blue-shifted in the metal complex (at 614 cm^{-1}). The band at 565 cm^{-1}corresponds exclusively to the complex and it was assigned to the δ(HOMg) bending mode. The FTIR absorption for the vibration mode of the water molecules is observed as a broad and intense band in the 3500-3000 cm^{-1} region, due to water νOH stretching modes, and also at ~1630 cm^{-1}, due to δ(HOH) bending mode (Fig. 5, Table S6).

The electronic spectra were also recorded and analyzed (Fig. 6). The UV spectrum of the free N,N-dimethylacetamide showed a very strong charge transfer (CT) band at 228 nm which is broader in the spectrum of MgDMA (not shown). In the reflectance spectra of the magnesium complex, there appear three bands, one at higher energy and intensity (206 nm) and the other two with lower intensity and located at 325 nm and 264 nm. A displacement of the most intense band of the solid complex is observed in the DMA spectrum. In free DMA, the very strong band at 228 nm is assigned to $\pi \rightarrow \pi^*$ transition. Though displaced, this band is also observed in the complex. The others, low-intensity, bands observed in the magnesium complex can be associated to the charged form of the ligand [11,30]. The calculations revealed the presence of the most intense bands (Fig. 6).

The electronic analysis indicated the molecular orbitals involved in the electronic transitions including the percentage of the main contributions (Fig. S1). H-1 HOMO and H-3 orbitals locate the electronic densities on the dimethylacetamide ligand, H-1 and H on nitrogen and methyl groups and H-3 on the oxygen atoms. LUMO distributes its electronic density on a coordinated water environment and L+1, L+2 and L+4 on the dimethylacetamide ligands. The main contributions are: for the band around ~200 nm: HOMO→LUMO (86%), H-1→LUMO (85%), H-3→L+1 (31%), H-3→L+2 (35%) and H-3→L+4 (16%) and for the band located at ~180 nm, H-1→L+1 (35%), HOMO→L+1 (33%), H-1→L+1 (39%), HOMO→L+1 (39%) and H-1→L+2 (11%). Calculations are in a reasonable agreement with the experimental data.

3.3. Phosphatase stimulation

Several studies concerning alkaline phosphatase (ALP) can be found in the literature. Some of them related to their inhibition, [31] others focus on similar activity, [32] and recently some of them associated with their activation [5,7].

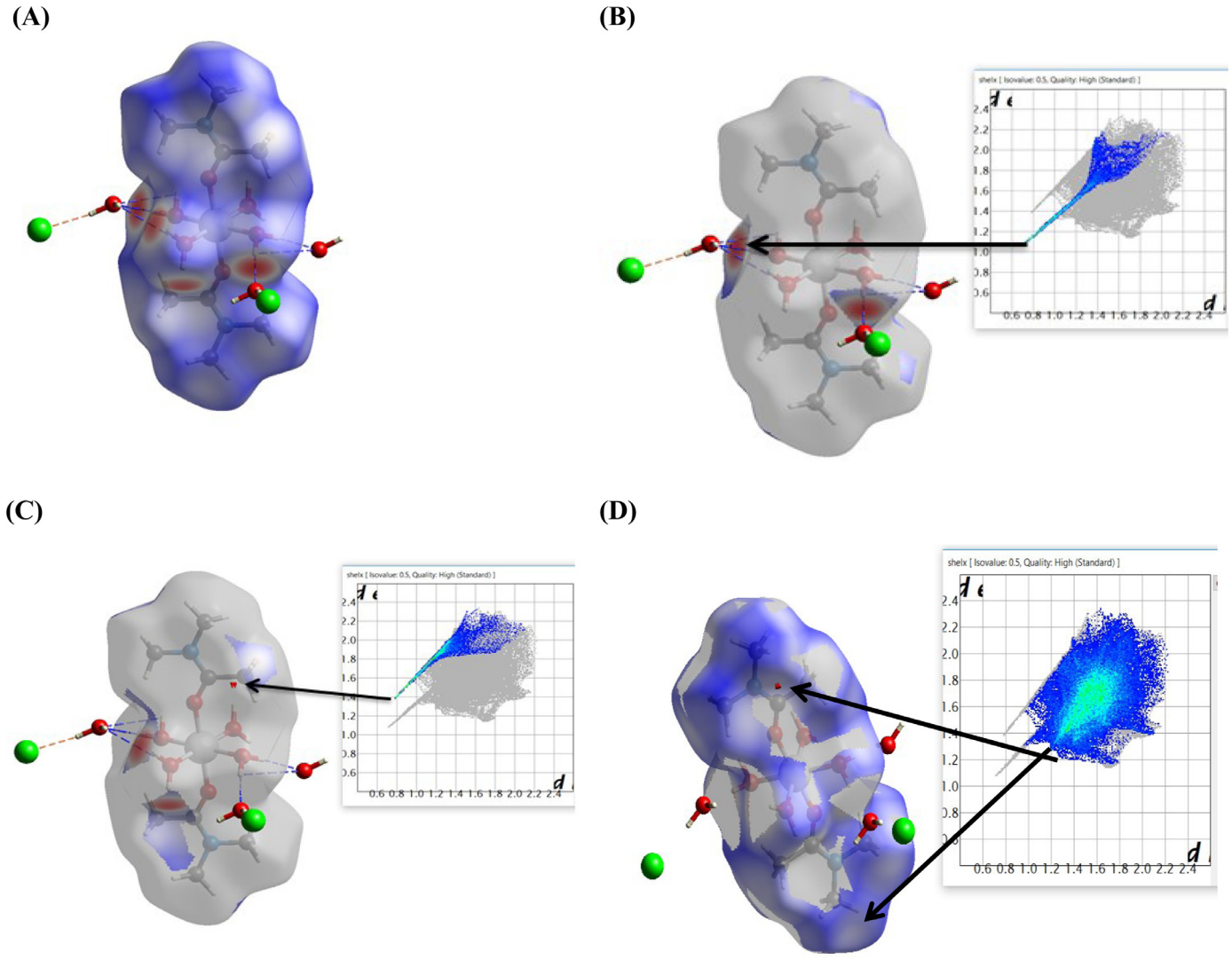

Fig. 4. Hirshfeld surfaces mapped with d_{norm} (A), the 2D fingerprint plots of: (B) H…..O, (C) H. . .Cl (D) H….H.

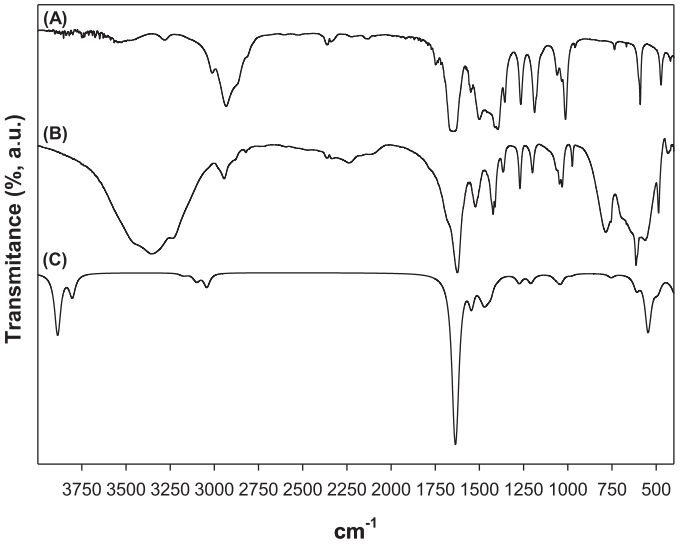

Fig. 5. Experimental FTIR spectra of (A) DMA and (B) $[Mg(DMA)_2(H_2O)_4]Cl_2.2H_2O$ and (C) calculated spectrum from $[Mg(DMA)_2(H_2O)_4]Cl_2.2H_2O$.

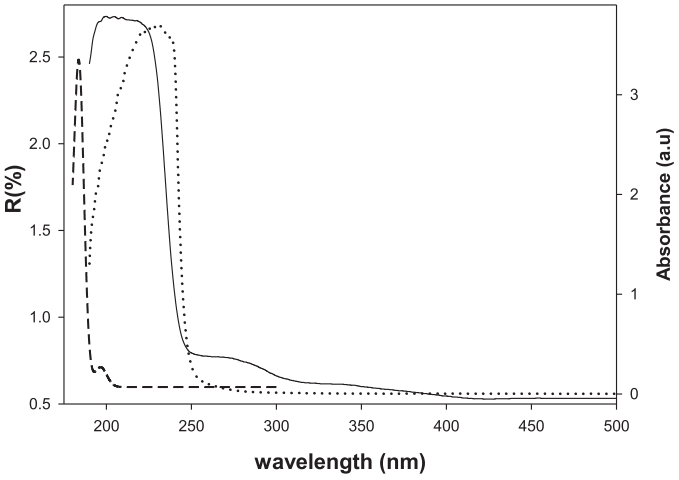

Fig. 6. Solid line, MgDMA, reflectance spectrum; Dashed line: calculated UV electronic spectrum for MgDMA; Dotted line: electronic spectrum for aqueous solution of DMA 0.26 M.

ALP is a marker of osteoblast differentiation, collagen synthesis, and osteoblast function. It is relevant in the formation of tissue and is highly expressed in mineralized tissue cells [33]. Studies regarding the anti-osteoporotic agent strontium ranelate (SR) showed that this compound was able to increase osteoblast bone formation and decrease osteoclastic bone resorption. It is known that SR acted increasing the alkaline phosphatase activity, the expression of osteoblast markers such as bone sialoprotein (BSP) and osteocalcin (OCN), resulting in an enhancement of the in vitro osteogenesis in osteoblast precursor and mature osteoblastic cells [34].

Magnesium acts as ALP cofactor and is also involved in the stimulation of bone mineralization acting as an essential bioelement [4,35]. Magnesium-related research refers to the strong regulation of Mg^{2+} on ALP of E. Coli [36]. Studies using the apoenzyme, showed an increment on enzyme activity in a 10:1 Mg^{2+}: enzyme ratio (veronal buffer) which was retained up to 30:1 ratio [37]. Because of that, several studies were carried on analyzing the interaction with other elements and pharmaceuticals. As it was mentioned, Fernández et al. [7] investigated the SR-Mg^{2+} interaction. Experiments on osteoblastic alkaline phosphatase demonstrate that the stimulatory effect of SR disappeared in the absence of Mg^{2+}, while in its presence, both SR and $SrCl_2$ increased ALP activity (15-66 %). Farrugia et al. [8] analyzed how a the combined administration of $NaVO_3$ and $MgSO_4$ affects bone mineralization, morphology and ALP levels in rats bone tissues. They used $MgSO_4$ instead $MgCl_2$ which is much less soluble than the chloride one (e.g. $MgSO_4.7H_2O$ (113 g/100 mL (20°C); $MgCl_2.6H_2O$ (235 g/100 mL (20°C)). The authors concluded that neither $NaVO_3$ nor $MgSO_4$ administration provoked significant changes in the ALP activity but the combined intake remarkably increase the levels of ALP by 40%.

Literature shows that different alkaline phosphatases could be affected by the presence of magnesium. It has also been shown that magnesium compounds may behave as anti-osteoporotic agents. [38] The activation of alkaline phosphatase could be a good strategy to develop a new class of anti-osteoporotic agents. Thus, we studied here the influence of the MgDMA compound on the enzyme activity, including experiments using $MgCl_2$ to compare their activities.

Table 4
ALP activity: kinetic parameters of ALP, ALP-Mg^{2+} and ALP-MgDMA systems and % of PNP at 10 min of reaction time.

	ALP	ALP-Mg^{2+}	ALP-MgDMA
V_{max} (mM.min^{-1})	1.34×10^{-3}	1.27×10^{-3}	1.73×10^{-3}
K_m (mM)	0.41	0.34	0.36
k_{cat} (min^{-1})	213.8	202.9	277.4
k_{cat}/K_m (M^{-1} min^{-1})	523.0	596.7	770.6
% PNP*	-	+6%	+53%
% Selectivity**	5	5.4	7.8

* Increment (%) of PNP concentration (PNPP = 0.4 mM) at 20 min of reaction time calculated in relation to that of the ALP.

** % Selectivity = moles of PNP/moles of PNPP x 100 at 20 min of reaction time at PNPP = 0.4 mM.

To evaluate the results, the Michaelis-Menten model was applied to get K_m constants to determine if MgDMA affects the affinity for PNPP.

The results are shown in Fig. 7 and Table 4. It is well-known that K_m constant reveals the enzyme affinity toward its substrate and a lower value of K_m means stronger affinity. It observed that the K_m value of the MgDMA complex is in the same order of magnitude than the value for Mg^{2+} alone, but the maximum velocity (V_{max}) substantially increased in the presence of the complex. By the analysis of the turnover numbers (k_{cat}) and catalytic efficiency (k_{cat}/K_m) values, it can be proposed that MgDMA stimulates efficiently the kinetic ability of ALP compared to the ALP with $MgCl_2$. (Table 4).

This stimulation process is correlated with the increment in the percentage of *p*-nitrophenol (PNP) at 20 minutes of the reaction time, which is 53% higher than the effect produced by ALP without the addition of MgDMA. In our experimental conditions, Mg^{2+} ions also increased PNP but the value is much lower than that for the complex.

The results also suggest that MgDMA is probably acting as a protector of enzyme degradation (Fig. 7A) because of the progressive decrease in the reaction speed measured for ALP in the absence of the complex.

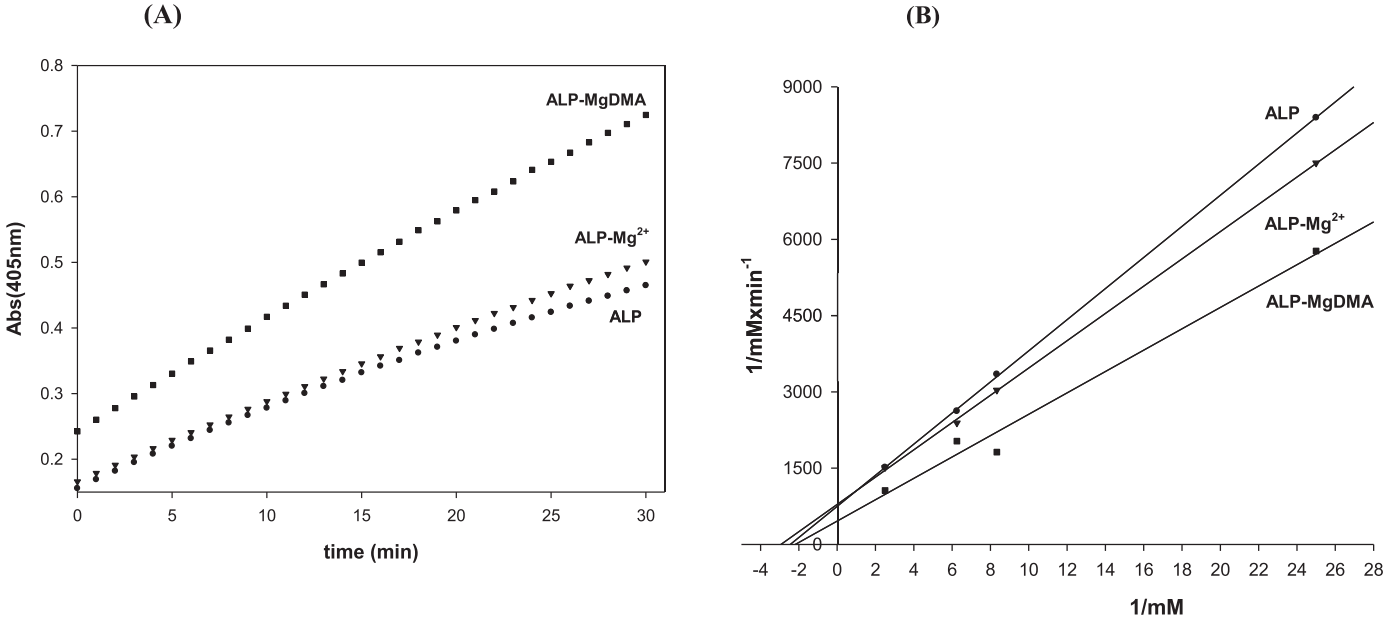

Fig. 7. (A) Absorbance vs time of p-nitrophenol (PNP) at 405 nm (ε=18500 M^{-1} cm^{-1}) in the ALP kinetic measurements. Concentrations: ALP = 6.25×10^{-5} mM; ALP (6.25×10^{-5} mM)-Mg^{2+}(5 mM) and ALP (6.25×10^{-5} mM)-MgDMA (5 mM) systems. PNPP = 0.4 mM. Data are the mean values from five experiments. **(B)** Lineweaver-Burk graph: $1/V = (K_m/V_{max})/[S] + 1/V_{max}$. Concentrations: ALP = 6.25×10^{-5} mM (correlation coefficient, r^2=0.99); ALP (6.25×10^{-5} mM)-Mg^{2+}(5 mM) (r^2 = 0.99) and ALP(6.25×10^{-5} mM)-MgDMA(5 mM) (r^2=0.98). Data are the mean values from five experiments.

Finally, it can be seen that the selectivity of ALP on PNPP increased by 1.5 times.

Unfortunately, a direct comparison with similar experiments (hydrolysis of p-NPP to p-nitrophenol (p-NP)) is not possible to perform due to the different sources of ALP used in the different tests. Nevertheless, some observations could be addressed.

Fernandez *et al.* found a K_m value of ~0.32 mM at an SR concentration of 0.5 mM which is similar to that obtained for MgDMA (5 mM).

On the other side, Vimalraj et al. studied a series of flavonoid-metal complexes that focus on the positive role of flavonoids on osteoblast differentiation and bone formation. They tested Zn-Morin complex, [39] ternary copper complexes with quercetin/neocuproine and phenanthroline [40] (Cells: MG-63 cells, concentration: 60 μM, time: 7 days), and ternary copper complexes with silibinin/neocuproine and phenanthroline (Cells: MG-63 cells, concentration: 60 μM, time: 3 days) [41]. Apparently, the [Cu(quer)(phen)], the [$Zn(morin)_2$] and the [Cu(sil)(phen)] complexes increased notably the ALP activity in almost 100%, 74% and 122%, respectively.

Bearing in mind our results and the information in literature, the synthesis and ALP stimulation of new metal-based materials is a promising development for the future, because of their favorable effect on osteoblast differentiation and angiogenesis.

Further studies are necessary to deepen the interpretation of its mechanism of action or to understand how it exerts the modification of the phosphatase structure favoring its efficiency.

3.4. Albumin binding

The interest of studying serum albumin binding is based on the extraordinary ability of this protein to act as a fundamental carrier of many drugs in the blood plasma. This is a fundamental aspect to determine the pharmacological activity of a drug because of its pharmacokinetic implications in its transport and delivery.

In this context, it was interesting to analyze the studies about the interaction of albumin and magnesium. With different methodologies, competitive Mg^{2+}-Ca^{2+}-binding have been studied using $MgCl_2$ and $CaCl_2$, and it was concluded that albumin did not make a difference in the binding of these ions [42,43] and that both cations have similar association constants (10^2-10^3) [13,44]. There is very usual to analyze the influence of metal cations in the binding of the substance of interest by fluorescence measurements. In this sense, Seedher *et al.* examined the interaction of magnesium and fluoroquinolone with human serum albumin (HSA). They reported that $MgCl_2$ (0.6-25 mM) did not provoked changes in its fluorescence intensity [14] and for that reason, they could not be determined Mg^{2+}-HSA association constant but demonstrated that the presence of Mg^{+2} reduced the binding of fluoroquinolones to HSA [14]. Mg^{2+} also reduced the association constant values of baicalein, [45] farrelol [46] and triamcinolone [47].

Conversely, in some experimental conditions, Mg^{2+} presence favors the interactions of albumin with bioligands, such as linoleic acid, [13] astragalin, [48] and genistein [49]. Again, the association constant between magnesium and BSA could not be determined [40].

Those results prompted us to investigate the interaction of MgDMA with BSA.

A comparison of the interaction of MgDMA with $MgCl_2$ was performed. This salt was used using the same experimental conditions. The results agree with those previously shown[14]. The ligand DMA did not change the intrinsic fluorescence intensity of the serum protein.

On the contrary, the magnesium complex showed interaction to some extent. To get a better insight of albumin interaction process, fluorescence measurements were performed at 25°C and 37°C using an excitation wavelength of 280 nm. The concentration of protein was fixed at 6 μM while that of the complex was varied in the range of 0-1000 μM. This concentration range was selected to make the results comparable to those used for magnesium chloride [14]. The addition of increasing concentrations of MgDMA complex provoked a slight and gradually quenching process on BSA fluorescence intensity until a concentration of 500 μM (Fig. S2). At higher concentrations, a saturation process is reached and no subsequent changes are observed. The quenching experiments showed a not very pronounced effect but one sufficient enough to estimate the Stern-Volmer constant, binding constants, and thermodynamic parameters (Table 5, Fig. S3). The obtained K_b values were in the order of those of magnesium salts obtained by other methodologies.

Thermodynamic data explained the prevalence of electrostatic interactions in the binding of magnesium to albumin [50]. Affinity chromatography experiments showed that at all pH values, the ΔH^o and ΔS^o values of the Mg^{2+}-HSA binding process were positive. They suggested an entropically driven process and refer to the fact that the interactions between ionic species in solution usually are characterized by small positive enthalpy and entropy changes [43,51]. Those results correlate with the proposed electrostatic attractions that occur between negatively charged non-specific regions of HSA and the positively charged Mg^{2+} ions.

The data obtained for MgDMA showed that the binding is a spontaneous process as suggested by the negative free energy change value (ΔG^0) accompanied by a positive ΔS^0 value. Thus, in a similar way than $MgCl_2$, the process seems to be entropically favored. Nevertheless, the ΔH^o and ΔS^o values are not comparable in magnitude (Table 5 and reference 42). In addition, the positive ΔH^0 value suggests an endothermic binding which is consistent with the increment of the K_b values [52].

The difference in interaction can be attributed to the incorporation of magnesium as a metal complex, as we will discuss below.

In general, the improvement or not of the binding process between the substance to be transported and the albumin cannot rule out the following considerations:

(i) metal complex interaction
(ii) dissociation or partial dissociation of the metal complex
(iii) allosteric mutual action
(iv) ligand or metal induced binding

Free magnesium, as it is supposed to be when incorporated as $MgCl_2$ displayed different types of effects on the interaction of drugs with albumin. Tannic acid (TA)-BSA interaction behavior was evaluated in the presence of Mg^{2+} by isothermal titration calorimetry (ITC) [53]. In this work, an excess of Mg^{2+}/BSA (650/1 molar:ratio) did not provoke remarkable changes in the thermodynamic parameters suggesting then that TA binds first to Mg^{2+} and then the complex binds to the BSA increasing affinity constant. Higher binding ability has not only been explained in terms of *in situ* metal-complex formation. Metals-induced conformational changes on albumin that result in a better affinity were also proposed [13,38]. The presence of Mg^{2+} improved linoleic acid (LA)-HSA-binding [13]. The authors proposed an allosteric effect in which the Mg^{2+} binding to HSA exposes additional binding sites for LA.

The experiments of displacement studies are not conclusive either. The interaction of the site-specific marker with the metal ion has not been studied. This interaction usually was not taken into account in the global analysis [39,40].

Finally, and regardless of the mode of interaction with albumin, the synergistic effect must be taken into account in the overall process.

UV/vis spectra were evaluated to obtain a more complete overview of the MgDMA-BSA interaction. In Fig. 8 (left) the spectra

Table 5
Stern Volmer constants (K_{sv}), apparent binding constants (K_b), "n" binding site and relative thermodynamic parameters for BSA-MgDMA interactions at different temperatures.

pH	T(K)	K_{sv} (M^{-1}) x 10^2 ± DS	K_b (M^{-1}) ± DS	n	r^{2a}	ΔG^0 (KJ/mol)	ΔH^0 (KJ/mol)	ΔS^0 (J/mol.K)
7.4	298	14.40 ± 0.02	39.81 ± 0.15	0.82	0.99	-9.17	172.4	609.3
	310	9.98 ± 0.50	588.8 ± 11.70	1.23	0.98			

DS: standard deviation.
[a] r^2 is the correlation coefficient for the K_b values.

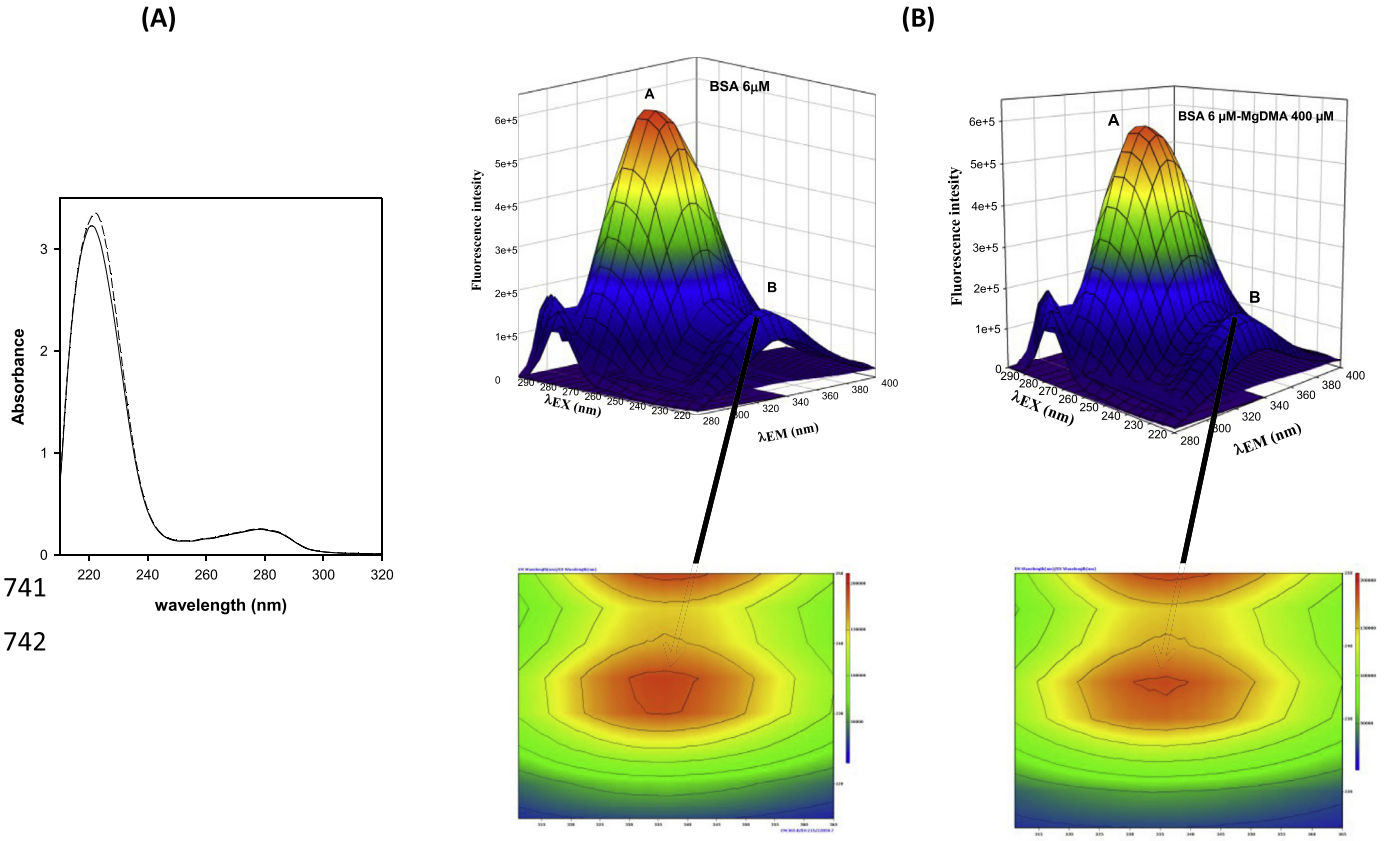

Fig. 8. Left. UV/vis spectra of BSA 6 μM (solid line) and BSA 6 μM-MgDMA 400 μM (Dash line); Right: three-dimensional fluorescence spectra of 6 μM BSA and BSA 6 μM-MgDMA 400 μM and the corresponding contour plots at λ_{em}: 365 nm; λ_{ex}: 215 nm.

of BSA 6 μM and the spectra of the system BSA 6 μM-MgDMA 400 μM are shown.

In the BSA spectrum, there is a strong absorption peak at 220 nm which is caused by the transition denoted as P→P* corresponding to the polypeptide backbone structure C=O related to the α-helix structure. This band increased the intensity and slightly red-shifts in presence of the complex. In opposition, no significant changes were observed in the band located at 280 nm which is correlated with the polarity of the microenvironment around the tryptophan (Trp) and tyrosine (Tyr) residues of albumin. These observations are in concordance with the weak quenching process observed and also with the fact that the magnesium complex does not change to a great extent the polarity of the microenvironment of the Trp and Tyr residues [54].

To gain a more complete picture of the interaction, the 3D fluorescence spectra were analyzed. Fig. 8 (right) presents the three-dimensional fluorescence spectra and contour map of BSA 6 μM and the BSA 6 μM-MgDMA 400 μM system. Peak A discloses the spectral behavior of the Trp and Tyr residues. Its fluorescence intensity is associated with the polarity of the microenvironment. Peak B is attributed to an n→π^* transition characteristic of the polypeptide backbone structure of the protein. The decrease in the intensity of the Peak B is more remarkable than the one of Peak A. This change is marked in the contour plot of Peak B with a decreasing of the area in the center of the eye (Fig. 8 (right)).

Based on these observations, it can be suggested that the addition of MgDMA to BSA induced a slight conformational change in the protein. The decrease in peak B correlates with a small unfolding of [55] the polypeptide strands affecting the secondary structure of the BSA (helix-coil structure).

The interaction of $MgCl_2$ with BSA seems to be different. According to the thermodynamic parameters ($\Delta H°$ and $\Delta S°$ are both positive) and the Ross and Subramanian considerations [56], the interaction may probably occur via a hydrophobic type.

It is worth mentioning that the binding of the compounds with HSA (human serum albumin) demonstrated to improve their bioactivity: (i) Gou *et al.* verified that the pre-incubation of Cu(II) compounds with HSA increased the mortality of cancer cells, [57] (ii) Caravan *et al.* showed that the residence time of gadolinium MRI contrast agent was incremented, [58] and (iii) Liboiron *et al.* proved the involvement of HSA with bis(maltolato)oxovanadium(IV) (BMOV) pro-

tected the complex against oxidation process and increased their efficacy [59].

The presence of Mg^{2+} forming a metal complex, MgDMA, led to a synergistic mechanism considering that neither free Mg^{2+} nor the ligand affected the intensity of fluorescence of the albumin. Thus, and due to the high solubility of MgDMA in water, it could be an optional candidate to be transported by albumin or for providing to the organism the magnesium requirements. Nevertheless, further specific studies are needed to elucidate them.

4. Conclusions

In this work, we develop a synthetic procedure for the preparation of a coordination complex containing magnesium and the very common pharmaceutical solvent N,N dimethylacetamide (DMA), formulated in the solid-state as $[Mg(DMA)_2(H_2O)_4]Cl_2.2H_2O$. This novel compound was characterized by several physicochemical techniques. The crystal structure was solved by X-ray diffraction methods and examined with Hirshfeld surface analysis (HSs). Optimization of the geometries afforded us to perform a complete vibration and electronic analysis that supports both the solid and solution characterization for in vitro pharmacological activities.

This study demonstrates a direct stimulation of ALP activity by the magnesium complex which is greater than that for $MgCl_2$.

Binding assays support the idea that the complex could be transported *via* the interaction through the polypeptide backbone structure of the protein.

Supplementary Information Available. Tables of fractional coordinates and equivalent isotropic displacement parameters of the non-H atoms (Table S1), full bond distances and angles (Table S2), atomic anisotropic displacement parameters (Table S3), hydrogen atoms positions (Table S4), and full H-bond distances and angles (Table S5). Crystallographic structural data have been deposited at the Cambridge Crystallographic Data Centre (CCDC). Any request to the Cambridge Crystallographic Data Centre for this material should quote the full literature citation and the reference number CCDC 1923111. Table S6. Observed and calculated wavenumbers with percentage of PED for $[Mg(DMA)_2(H_2O)_4]Cl_2.2H_2O$ and DMA assignments from ref [29]. Fig. S1. Calculated electronic UV-Vis assignments. Fig. S2. Fluorescence spectra**.** Fig. S3. Stern Volmer plots (F^0/F vs [MgDMA]) and log [(F^0-F)/F] vs log [MgDMA].

Declaration of Competing Interest

The authors declare that they have no conflict of interest.

CRediT authorship contribution statement

Nancy Martini: Methodology, Investigation, Formal analysis, Validation. **Juliana E. Parente:** Methodology, Investigation, Formal analysis, Validation. **Gonzalo Restrepo-Guerrero:** Methodology, Investigation, Formal analysis, Validation. **Carlos A. Franca:** Software, Formal analysis, Validation. **Oscar E. Piro:** Investigation, Validation, Formal analysis. **Gustavo A. Echeverría:** Investigation, Validation, Formal analysis. **Patricia A.M. Williams:** Writing - review & editing, Project administration, Funding acquisition, Resources. **Evelina G. Ferrer:** Conceptualization, Writing - original draft, Writing - review & editing, Visualization, Supervision, Project administration, Funding acquisition, Resources.

Acknowledgments

This work was supported by CONICET (Grants PIP 0611 and PIP 0651), ANPCyT (Grant PICT16-1814), UNLP (Grants 11/X777 and 11/X709) of Argentina. LGN, EGF, GAE and OEP are Research Fellows of CONICET. JEP and PAMW are Research Fellows of CICPBA, Argentina.

Supplementary materials

Supplementary material associated with this article can be found, in the online version, at doi:10.1016/j.molstruc.2020.129240.

References

[1] W. Jahnen-Dechent, M Ketteler, Magnesium basics, Clin. Kidney J. 5 (2012) i3–i14, doi:10.1093/ndtplus/sfr163.
[2] M. Firoz, M. Graber, Bioavailability of US commercial magnesium preparations, Magnesium Res. 14 (2001) 257–262.
[3] E.E. Golub, K. Boesze-Battaglia, The role of alkaline phosphatase in mineralization, Curr. Opin. Orthop. 18 (2007) 444–448, doi:10.1097/BCO.0b013e3282630851.
[4] A. Ścibior, A. Adamczyk, R. Mroczka, I. Niedźwiecka, D. Gołębiowska, E. Fornal, Effects of vanadium (V) and magnesium (Mg) on rat bone tissue: mineral status and micromorphology.Consequences of V–Mg interactions, Metallomics 6 (2014) 2260–2278, doi:10.1039/C4MT00234B.
[5] N. Mazaheri, N. Naghsh, A. Karimi, H. Salavati, In vivo toxicity investigation of magnesium oxide nanoparticles in rat for environmental and biomedical applications, Iran. J. Biotech. 17 (2019) 1–9 e1543, doi:10.21859/IJB.1543.
[6] R.L. Dean, Kinetic studies with alkaline phosphatase in the presence and absence of inhibitors and divalent cations, Biochem. Mol. Biol. Educ. 30 (2002) 401–407, doi:10.1002/bmb.2002.494030060138.
[7] J.M. Fernández, M.S. Molinuevo, A.D. McCarthy, A.M. Cortizo, Strontium ranelate stimulates the activity of bone-specific alkaline phosphatase: interaction with Zn^{2+} and Mg^{2+}, Biometals 27 (2014) 601–607, doi:10.1007/s10534-014-9733-8.
[8] G. Farruggia, S. Castiglioni, A. Sargenti, C. Marraccini, A. Cazzaniga, L. Merolle, S. Iotti, C. Cappadone, J.A.M. Maier, Effects of supplementation with different Mg salts in cells: is there a clue? Magnesium Res. 27 (2014) 25–34, doi:10.1684/mrh.2014.0359.
[9] S-N Kim, Preclinical toxicology and Pharmacology of dimethylacetamide, with clinical notes, Drug Metabol. Rev. 19 (1988) 345–368, doi:10.3109/036025388089941.
[10] W.E. Bull, S.K. Madan, J.E. Willis, Amides as ligands I. Metallic complexes of N,N-Dimethylacetamide, Inorg. Chem. 2 (1963) 303–306, doi:10.1021/ic50006a016.
[11] K.S. Dahl, D.C. Luehrs, Dimethylacetamide solvates of alkali Metal salts, Z. Inorg. Nucl. Chem. 38 (1976) 1773–1774, doi:10.1016/0022-1902(76)80085-1.
[12] L. Pavanello, P. Visoria, S. Bresadola, Synthesis and X-ray structure of hexakis (N,N-dimethylacetamide-O)magnesium tetrachloromagnesate, Z. Kristallog. 209 (1994) 946–949, doi:10.1524/zkri.1994.209.12.946.
[13] E.L. Nemashkalova, E.A. Permyakov, S.E. Permyakov, E.A. Litus, Modulation of linoleic acid-binding properties of human serum albumin by divalent metal cations, Biometals 30 (2017) 341–353, doi:10.1007/s10534-017-0010-5.
[14] N. Seedher, P. Agarwal, Effect of metal ions on some pharmacologically relevant interactions involving fluoroquinolone antibiotics, Drug Metab. Drug Interact. 25 (2010) 17–24, doi:10.1515/DMDI.2010.003.
[15] CrysAlisPro, Oxford Diffraction Ltd., version 1.171.33.48 (release 15-09-2009 CrysAlis171.NET).
[16] G.M. Sheldrick, SHELXT Integrated space-group and crystal-structure determination, Acta Cryst. A71 (2015) 3–8, doi:10.1107/S2053273314026370.
[17] G.M. Sheldrick, A short history of SHELX, Acta Crystallogr. A64 (2008) 112–122, doi:10.1107/S0108767307043930.
[18] S.K. Wolff, D.J. Grimwood, J.J. McKinnon, M.J. Turner, D. Jayatilaka, M.A. Spackman, CrystalExplorer 3.1. University of Western Australia, Crawley, Western Australia, 2005-2013, http://hirshfeldsurface.net/CrystalExplorer.
[19] M.J. Frisch, G.W. Trucks, H.B. Schlegel, G.E. Scuseria, M.A. Robb, J.R. Cheeseman, V.Barone G.Scalmani, B. Mennucci, G.A Petersson., H. Nakatsuji, M. Caricato, X. Li, H.P. Hratchian, A.F. Izmaylov, J. Bloino, G. Zheng, J.L. Sonnenberg, M. Hada, M. Ehara, K. Toyota, R. Fukuda, J. Hasegawa, M. Ishida, T. Nakajima, Y. Honda, O. Kitao, H. Nakai, T. Vreven, J.J.A. Montgomery, J.E. Peralta, F. Ogliaro, M. Bearpark, J.J. Heyd, E. Brothers, K.N. Kudin, V.N. Staroverov, T. Keith, R. Kobayashi, J. Normand, K. Raghavachari, A. Rendell, J.C. Burant, S.S. Iyengar, J. Tomasi, M. Cossi, N. Rega, J.M. Millam, M. Klene, J.E. Knox, J.B. Cross, V. Bakken, C. Adamo, J. Jaramillo, R. Gomperts, R.E. Stratmann, O. Yazyev, A.J. Austin, R. Cammi, C. Pomelli, J.W. Ochterski, R.L. Martin, K. Morokuma, V.G. Zakrzewski, G.A. Voth, P, Salvador, J.J. Dannenberg, S. Dapprich, A.D. Daniels, O. Farkas, J.B. Foresman, J.V. Ortiz, J. Cioslowski, D.J. Fox, Gaussian-09, Gaussian Inc., Wallingford, 2010.
[20] A.D. Becke, Density-functional exchange-energy approximation with correct asymptotic behavior, Phys. Rev. A 38 (1988) 3098–3100, doi:10.1103/PhysRevA.38.3098.
[21] R.G. Parr, Density functional theory of atoms and molecules, in: K Fukui, B Pullman (Eds.), Horizons of Quantum Chemistry. Académie Internationale Des Sciences Moléculaires Quantiques/International Academy of Quantum Molecular Science, 3, Springer, Dordrecht, 1980, doi:10.1007/978-94-009-9027-2_2.
[22] M.J. Frisch, J.A. Pople, J.S. Binkley, Self-consistent molecular orbital methods. Supplementary functions for Gaussian basis sets, J. Chem. Phys. 80 (1984) 3265–3269, doi:10.1063/1.447079.
[23] K. Wolinski, J.F. Hinton, P Pulay, Efficient implementation of the gauge-independent atomic orbital method for NMR chemical shift calculations, J. Am. Chem. Soc. 112 (1990) 8251–8260, doi:10.1021/ja00179a005.

[24] M.E. Casida, C. Jamorski, K.C. Casida, D.R. Salahub, Molecular excitation energies to high-lying bound states from time-dependent density-functional response theory: Characterization and correction of the time-dependent local density approximation ionization threshold, J. Chem. Phys. 108 (1988) 4439–4449, doi:10.1063/1.475855.
[25] V. Barone, M. Cossi, Quantum calculation of molecular energies and energy gradients in solution by a conductor solvent model, J. Phys. Chem. A 102 (1988) 1995–2001, doi:10.1021/jp9716997.
[26] N. Martini, J.E. Parente, M.E. Toledo, G.E. Escudero, C.H. Laino, J.J. Martínez Medina, G.A. Echeverría, O.E. Piro, L. Lezama, P.A.M. Williams, E.G. Ferrer, Evidence of promising biological-pharmacological activities of the sertraline-based copper complex: $(SerH_2)_2[CuCl_4]$, J. Inorg. Biochem. 174 (2014) 76–89, doi:10.1016/j.jinorgbio.2017.05.012.
[27] L.J. Farrugia, ORTEP-3 for windows -a version of ORTEP-III with a graphical user interface (GUI), J. Appl. Cryst. 30 (1997) 565–566, doi:10.1107/S0021889897003117.
[28] S. Grabowsky, P.M. Dean, B.W. Skelton, A.N. Sobolev, M.A. Spackmana, A.H. White, Crystal packing in the 2-R,4-oxo-[1,3-a/b]-naphthodioxanes-Hirshfeld surface analysis and melting point correlation, CrystEngComm 14 (2012) 1083–1093, doi:10.1039/C2CE06393J.
[29] G. Durgaprasad, D.N. Sathyanarayana, C.C. Patel, Normal vibrations of N,N-dimethylacetamide, Spectrochim. Acta 28 (1972) 2311-1318, doi:10.1016/0584-8539(72)80211-3.
[30] E. Benedetti, B. Di Blasio, P. Baine, Structure, and infrared and ultraviolet spectra of protonated dimethylacetamide, J. Chem. Soc. Perkin Trans. 2 (1980) 500–503, doi:10.1039/P29800000500.
[31] M. al-Rashida1, J. Iqbal, Inhibition of alkaline phosphatase: an emerging new drug target, Mini-Rev. Med. Chem. 15 (2015) 41–54, doi:10.2174/1389557515666150219113205.
[32] N. Dutta, S. Haldar, G. Vijaykumar, S. Paul, A.P. Chattopadhyay, L. Carrella, M. Bera, Phosphatase-like activity of tetranuclear iron(III) and zinc(II) complexes, Inorg. Chem. 57 (2018) 10802–10820, doi:10.1021/acs.inorgchem.8b01441.
[33] E. E. Golub, K. Boesze-Battaglia, The role of alkaline phosphatase in mineralization, Curr Opin Orthop.18:444-448, doi: 10.1097/BCO.0b013e3282630851.
[34] Z. Saidak, P.J. Marie, Strontium signaling: molecular mechanisms and therapeutic implications in osteoporosis, Pharmacol. Therapeut. 136 (2012) 216–226, doi:10.1016/j.pharmthera.2012.07.009.
[35] W.C. Lu, E. Pringa, L. Chou, Effect of magnesium on the osteogenesis of normal human osteoblasts, Magnes. Res. 30 (2017) 42–52, doi:10.1684/mrh.2017.0422.
[36] W.F. Bosron, R.A. Anderson, M.C. Falk, F.S. Kenedy, B.L. Vallee, Effect of magnesium on the properties of zinc alkaline phosphatase, Biochemistry 16 (1977) 610–614, doi:10.1021/bi00623a009.
[37] D.J. Plocke, B.L. Vallee, Interaction of alkaline phosphatase of *E. coli* with metal ions and chelating agents, Biochemistry 1 (1962) 1039–1043, doi:10.1021/bi00912a014.
[38] Y. Li, J. Yue, C. Yang, Unraveling the role of Mg^{++} in osteoarthritis, Life Sci. 147 (2016) 24–29, doi:10.1016/j.lfs.2016.01.029.
[39] S. Vimalraja, S. Rajalakshmi, S. Saravananc, T. Deepak, K. Murugand, A.Vasanthi Rajkumare, D. Anuradha, Zinc chelated morin promotes osteoblast differentiation over its uncomplexed counterpart, Process Biochem. 82 (2019) 167–172, doi:10.1016/j.procbio.2019.04.008.
[40] S. Vimalraja, S. Rajalakshmi, D.R. Preeth, S.V. Kumarc, T. Deepak, V. Gopinath, K. Murugan, S. Chatterjee, Mixed-ligand copper(II) complex of quercetin regulate osteogenesis and angiogenesis, Mater. Sci. Eng. C 83 (2018) 187–194, doi:10.1016/j.msec.2017.09.005.
[41] S. Rajalakshmi, S. Vimalraj, S. Saravanan, D.R. Preeth, M. Shairam, D. Anuradha, Synthesis and characterization of silibinin/phenanthroline/ neocuproine copper(II) complexes for augmenting bone tissue regeneration: an in vitro analysis, JBIC 23 (2018) 753–762, doi:10.1007/s00775-018-1566-4.
[42] K.O. Pedersen, Binding of calcium to serum albumin. III. Influence of ionic strength and ionic medium, Scand. J. Clin. Lab. Invest. 29 (1972) 427–432, doi:10.3109/00365517209080262.
[43] C. Carr, Competitive binding of calcium and magnesium with serum albumin, Proc. Soc. Exp. Biol. Med. 89 (1955) 546–549, doi:10.3181/00379727-89-21870.
[44] K.A. Majorek, P.J. Porebski, A. Dayal1, M.D. Zimmerman, K. Jablonska, A.J. Stewart, M. Chruszcz, W. Minor, Structural and immunologic characterization of bovine, horse, and rabbit serum albumins, Mol. Immunol. 52 (2012) 174–182, doi:10.1016/j.molimm.2012.05.011.
[45] A.S. Roy, A.K. Dinda, N.K. Pandey, S. Dasgupta, Effects of urea, metal ions and surfactants on the binding of baicalein with bovine serum albumin, J. Pharm. Anal. 6 (2016) 256–267, doi:10.1016/j.jpha.2016.04.001.
[46] D. Li, Y. Wang, J. Chen, B. Ji, Characterization of the interaction between farrerol and bovine serum albumin by fluorescence and circular dichroism, Spectrochim. Acta Part A 79 (2011) 680–686, doi:10.1016/j.saa.2011.04.005.
[47] S. Siddiqui, F. Ameen, I. Jahan, S.M. Nayeem, M. Tabish, A comprehensive spectroscopic and computational investigation on the binding of the anti-asthmatic drug triamcinolone with serum albumin, New J. Chem. 43 (2019) 4137–4151.
[48] S.L. Lyu, W Wang, Spectroscopic methodologies and computational simulation studies on the characterization of the interaction between human serum albumin and Astragalin, J. Biomol. Struct. Dyn. 29 (2020) 1–12, doi:10.1080/07391102.2020.1758213.
[49] A.S. Roy, D.R. Tripathy, A. Chatterjee, S. Dasgupta, The influence of common metal ions on the interactions of the isoflavone genistein with bovine serum albumin, Spectrochim. Acta Part A: Mol. Biomol. Spectrosc. 102 (2013) 393–402, doi:10.1016/j.saa.2012.09.053.
[50] Y.C. Guillaume, C. Guinchard, A. Berthelot, Affinity chromatography study of magnesium and calcium binding to human serum albumin: pH and temperature variations, Talanta 53 (2000) 561–569, doi:10.1016/S0039-9140(00)00536-1.
[51] Y.C. Guillaume, E. Peyrin, A. Berthelot, Chromatographic study of magnesium and calcium binding to immobilized human serum albumin, J. Chromatogr B 728 (1999) 167–174, doi:10.1016/s0378-4347(99)00117-6.
[52] V.D. Suryawanshi, L.S. Walekar, A.H. Gore, P.V. Anbhule, G.B. Kolekar, Spectroscopic analysis on the binding interaction of biologically active pyrimidine derivative with bovine serum albumin, J. Pharm. Anal. 6 (2016) 56–63, doi:10.1016/j.jpha.2015.07.001.
[53] E. Kaspchak, A.C. Goedert, L. Igarashi-Mafra, M.R. Mafra, Effect of divalent cations on bovine serum albumin (BSA) and tannic acid interaction and its influence on turbidity and in vitro protein digestibility, Int. J. Biol. Macromol. 136 (2019) 486–492, doi:10.1016/j.ijbiomac.2019.06.102.
[54] D. Li, M. Zhu, C. Xu, B. Ji, Characterization of the baicaleine bovine serum albumin complex without or with Cu^{2+} or Fe^{3+} by spectroscopic approaches, Eur. J. Med. Chem. 46 (2011) 588–599, doi:10.1016/j.ejmech.2010.11.038.
[55] Y. Wang, X. Wang, J. Wang, Y. Zhao, W. He, Z. Guo, Noncovalent interactions between a trinuclear monofunctional platinum complex and human serum albumin, Inorg. Chem. 50 (2011) 12661–12668, doi:10.1021/ic201712e.
[56] P. Ross, S. Subramanian, Thermodynamics of protein association reactions: forces contributing to stability, Biochemistry 20 (1981) 3096–3102, doi:10.1021/bi00514a017.
[57] Y. Gou, Y. Zhang, J. Qi, Z. Zhou, F. Yang, H. Liang, Enhancing the copper(II) complexes cytotoxicity to cancer cells through bound to human serum albumin, J. Inorg. Biochem. 144 (2015) 47–55, doi:10.1016/j.jinorgbio.2014.12.012.
[58] P. Caravan, N.J. Cloutier, M.T. Greenfield, S.A. McDermid, S.U. Dunham, J.W.M. Bulte, J.C. Amedio Jr., R.J. Looby, R.M. Supkowski, W.D. Horrocks Jr., T.J. McMurry, R.B. Lauffer, J. Am. Chem. Soc. 124 (2002) 3152–3162, doi:10.1021/ja017168k.
[59] K.H. Thompson, C. Orvig, Metal complexes in medicinal chemistry: new vistas and challenges in drug design, Dalton Trans. (2006) 761–764, doi:10.1039/b513476e.